Step towards Enriching Frequency Support from Wind-Driven Permanent-Magnet Synchronous Generator for Power System Stability

Muhammad Arif Sharafat ALI
Department of Electrical and Computer Engineering,
Sungkyunkwan University, Natural Sciences Campus, Suwon 440-746, Republic of Korea
sharafat@skku.edu

***Abstract*—Wind power plants do not provide frequency support subject to disturbances because wind turbine generators (WTGs) are decoupled from system frequency deviations. To provide frequency regulation from a permanent-magnet synchronous generator-based wind energy conversion system following the change in system load demand, this paper presents a basic controller that directly perturbs the rotor-speed reference according to system frequency deviations. In the proposed approach, the kinetic energy (KE) of the rotating parts of the WTGs is utilized for frequency support, thus enriching the power system stability. The prominent aspect of opting for this concept is the immediate KE release or absorption through a step-change in the speed reference. Furthermore, the system proceeds to its normal operation without causing instability issues. To prove this concept, extensive simulations in MATLAB/Simulink have been performed, and the results demonstrate its good capability in providing system frequency regulation, resulting in the enhancement of power system stability. For comparison, simultaneous control of the power-frequency droop control and DC-link inertial support was also prepared.**

***Index Terms*—frequency, generators, kinetic energy, power system stability, wind energy integration.**

I. INTRODUCTION

The increased share of wind generators in power systems has posed new challenges for power system operators in the context of not participating in system frequency regulation and contributing to reduced inertial responses as wind turbines (WTs) and power grid connections are made via power electronic interfaces (PEIs) [1], which decouple the rotational speed of the WT rotor and the system frequency [2-6]. Thus, this property effectively prevents WTs from responding to system frequency deviations [7-9]. Present WTs commonly follow maximum power tracking operations to extract the maximum possible energy from wind [10-12]. In this regard, the wind turbine generator (WTG) seems 'immune' to grid frequency disturbances. With increased penetration of wind power, wind power plants (WPPs) are expected to operate like conventional power plants in providing frequency and voltage control supports.

In the absence of rotating bodies, PEI provides low inertia, which is a leading cause of poor voltage and frequency response against system disturbances. It jeopardizes the stability of the power systems [13]. Concerning the shortage of inertia and poor frequency support capability, it is possible to develop a frequency regulation control by modifying WTG controls such that the stored kinetic energy (KE) of the WTGs can be utilized. The dynamic response of the system frequency subject to a disturbance is improved by utilizing the WTG's self-potential. However, it should be sufficient to satisfy the basic performance under diversified wind-speed conditions.

To highlight the motivation behind this study, a critical review of the state-of-the-art techniques available in the literature for frequency and inertial emulation schemes is presented. To counter the problem of poor frequency regulation against sudden changes in system load demands, several articles have been published so far that have proposed technical solutions based on modified WTG controls and auxiliary hardware support. Modified WTG controls involve wind energy conversion systems (WECSs) to utilize their potential to enhance the frequency response against sudden changes in system demand. Revised WTG control-based solutions can be grouped into three main types: pitch-angle control (PAC)-based methods, methods utilizing the KE of WTG, and miscellaneous methods. The first type employs the pitch control action of the WT to regulate the captured wind energy [14-15]. The WT-reserved energy can be utilized to support the system frequency employing the pitch action. However, the response of PAC is sluggish owing to the mechanical dynamics of the WT. The excessive operation of blade pitching can increase the mechanical stresses on the WTG and can cause WT fatigue.

In contrast, the second type of solution utilizes the stored KE of the rotating masses of the WECS to contribute to frequency regulation via properly designed inertial controls. The core idea behind this type is to regulate the power set reference according to the system measured frequency and release or absorbs the KE by decelerating or accelerating the rotor speed. Compared to the PAC, the fast response and surplus energy stored in the rotating masses are significant advantages of inertial emulation controls based on utilizing KE. This type can be further divided into three classes based on their implementation modes: power-frequency droop controllers, derivative controllers, and de-loading controllers.

A power-frequency droop controller provides continuous active power in response to the measured frequency, exceeding its defined limits [16-19]. Although the literature reported a good response in providing frequency support, it may lead to system wear and tear due to high droop values,

Digital Object Identifier 10.4316/AECE.2022.01009

which eventually increases the maintenance issues. A derivative controller triggers a synchronous generator (SG) inertial-like response [18], [20-21]. Despite achieving a good inertial response, the derivative controllers may cause system instability issues owing to the derivative term, which could cause noise in the frequency measurement. Furthermore, the WTG cannot provide frequency support when exceeding its limits if only the derivative controller is applied. A de-loading controller assists variable-speed WTs (VSWTs) to obtain a reserve power margin [22-24]. In this method, the maximum power point tracking (MPPT) operation is shifted to the right sub-optimal curve. The significant disadvantage of using a de-loading operation is the wind-energy loss, which is unavoidable.

The use of DC-link energy in supporting system inertia has also been reported in the literature [25-27]. When an abnormality in the system's frequency is detected, the DC-link voltage reference is altered to absorb or release its stored energy. However, the influence of DC-link in providing inertial support is relatively small owing to the capacitor size. In [28], the authors proposed a simultaneous coordinated control involving the use of stored KE of the WTG and DC-link energy so that the frequency response of the permanent-magnet synchronous generator (PMSG)-based WT system can be improved. The authors of [29] proposed a modified virtual synchronous generator control scheme to expand the stable operational limits of doubly-fed induction generators (DFIG) and thus prevent grid frequency deviations. A coordinated control method for the DFIG was proposed in [30] using virtual inertia and primary frequency control, in which a portion of the wind power is reserved by PAC and over-speed control to compensate for the decrease in wind power after a transient power surge. Various technical concepts, such as virtual synchronous machines [31-32] and synchronverters [33], have been reported to minimize the system's frequency deviations by improving the inverter control designs. In these concepts, the rotor speed is regulated to minimize the maximum deviation of the nearby WTG.

A potential solution for enhancing the system transient performance is utilizing energy storage devices (ESDs), such as batteries and supercapacitors in WTG control systems [34-40]. Unfortunately, when considering the disturbance location in a large and interconnected power system, ESD-based solutions may become costly and ineffective.

In this study, a concept based on the direct perturbation of the rotor-speed reference using the system frequency deviation is proposed. In this regard, a basic controller based on momentarily utilizing the KE of the WTGs is developed, aiming to enhance the power system stability and to provide frequency support subject to a disturbance. Simplicity, fast response, and excellent performance are significant advantages of the proposed concept. Furthermore, the WTGs are returned to their normal operations without initiating unnecessary system stresses or instability issues. Given the above benefits, the proposed concept is suitable and attractive for wind energy applications.

The remainder of this paper is organized as follows. Section II presents the proposed control design with detailed mathematical modelling and analyses, aiming to enhance the frequency support from a wind-driven PMSG under system disturbances. In Section III, numerical simulation results for a power system are presented and discussed to verify the proposed concept according to system disturbances under various wind speed conditions. Section IV summarizes the conclusions of the study.

II. Proposed Frequency Support Scheme

This section explains the proposed control concept aimed at improving the frequency support of a wind-driven PMSG under system disturbances. In this regard, the provision of the inertial response of the WTG is presented. The proposed control concept for providing frequency support was then explained using detailed mathematical modelling and analyses.

A. WTG Inertial Provision

A significant amount of KE is stored in the rotating masses of a PMSG-based WTG to support the grid frequency characteristics by making suitable modifications to the WTG converter controls. Equation 1 describes the rotor speed (ω_r) of an SG.

$$J_T \frac{d}{dt}\omega_r = T_t - T_e \tag{1}$$

In the normal operating mode, the stored KE will be constant because of the balance between the turbine power and load power, which is expressed as:

$$KE = 0.5 J_T \omega_{r,rated}^2 \tag{2}$$

The inertial power (P_{KE}) contributions available from an SG can be determined by taking the derivative of the KE stored in the rotating parts and is given by:

$$P_{KE} = \frac{d}{dt} KE = J_T \omega_r \frac{d}{dt}\omega_r \tag{3}$$

When the balance is disturbed, following the generation loss, ($T_t - T_e$) becomes negative. As a result, the rotor speed decelerates, and the frequency decreases. In this scenario, the power deficiency is covered by stored KE. It is a well-known fact that whenever the system frequency deviates from a disturbance, mechanical power cannot change instantly. Thus, the electric power acts to change the rotor speed to counter frequency changes.

To this point, the emphasis is placed on synchronously connected generators. Now, the focus is shifted toward the delivery of the inertial response from the VSWT. As mentioned earlier, the WT output power is insensitive to the system frequency because of PEI. In contrast, there exists a facility that imitates the inertial response from a VSWT by regulating power reference against frequency changes. It can be triggered by revising the WTG controls in response to frequency changes, which adds an extra power-reference term (ΔP_{KE}) that regulates the generator output power.

$$P_{ref}^* = P_{ref} + \Delta P_{KE} \tag{4}$$

The role of stored KE in WTG is significant in frequency support, particularly in massive wind power penetration. It is noteworthy that the stored energy depends on wind speed, and it will vary at different wind speeds. Further, the rotor speed does not differ at a constant rate despite a fixed rate of change in the system frequency because WTGs are not synchronously connected to the system. The rotor speed of

the WTG also depends on the wind speed. Therefore, any change in wind speed causes an imbalance between the turbine torque and generator torque, which ultimately accelerates or decelerates the rotor speed. Notably, the WTGs are normally equipped with MPPT controllers embedded into the turbine controllers to ensure turbine operation effectively by harvesting the maximum possible energy from wind.

To counter the torque imbalance situation, the turbine controller will act to bring the WT back by regulating the rotor speed and will achieve the balance again. The MPPT operation is activated when the WT operates below the rated wind speed, and in this context, the following relation holds:

$$P_{ref} = K_{opt}\omega_r^3 \tag{5}$$

where

$$K_{opt} = 0.5\rho\pi R^5 \frac{C_{p,opt}}{\lambda_{opt}^3}$$

To limit the rotor speed above the rated wind speed, PAC is activated to regulate the wind power and ensure that the power constraint is not violated.

B. Proposed Concept for Frequency Support

The proposed concept also involves utilizing the KE stored in the WTG subject to frequency changes. However, it differs in the context in which the inertial response is triggered by the direct control of the rotor-speed reference ($\omega_{r\text{-}ref}$) in response to frequency deviations when exceeding the preset limits. In the proposed design, also referred to as the $\omega_{r\text{-}ref}$ - f controller, the controller delivers a reference speed signal ($\Delta\omega_{r\text{-}ref}$) based on system frequency changes, which is added to the speed reference signal ($\omega_{r\text{-}ref}$) realized by the MPPT controller expressed in Equation (6).

$$\omega_{r-ref} = \frac{P_{gen}}{P_{g,rated}}\omega_{r,rated} \tag{6}$$

Whenever a frequency deviation exceeds its predefined limits, the stored KE quickly changes following the deviation and satisfies the power deficiency. In this regard, the modified speed reference becomes:

$$\omega_{r-ref}^* = \omega_{r-ref} + \Delta\omega_{r-ref} \tag{7}$$

The first term on the right-hand side of Equation (7) is mostly present in the VSWTs, which ensures WECS performance under normal conditions. In comparison, the effect of the second term of Equation (7) is evident whenever an inertial response is required in response to a frequency deviation. As a result, the overall speed reference will be a variable quantity even under constant wind-speed conditions because of two facts: the first is due to the system frequency deviations when it goes beyond its thresholds and modifies the output of the proposed controller. In contrast, the second fact is related to the speed reference realized from MPPT, which is also a variable quantity under the influence of the first one. The grid nominal and measured frequencies are compared, and the difference is added to the output of the MPPT controller after multiplying it by a factor of K_ω.

$$\Delta\omega_{r-ref} = K_\omega \Delta f_g \tag{8}$$

where

$$\Delta f_g = f_g - f_{g,meas}$$

The factor K_ω is a decisive parameter in determining the stability of the PMSG-WTG under the proposed design, as it directly influences the inertial control in providing frequency support. It is advantageous to add an extra rotor-speed reference term directly into the WTG control because, in this way, the power regulation and speed regulation can be accomplished simultaneously. Furthermore, it prevents the rotor from dropping below its lower limit.

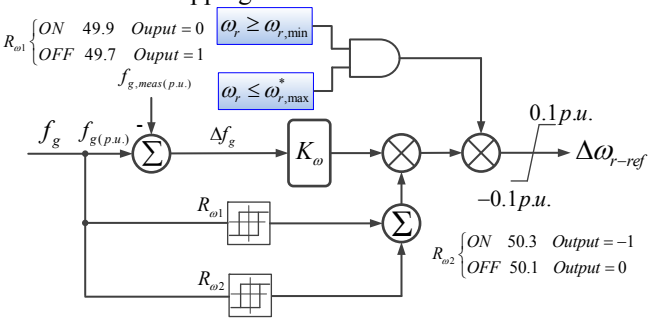

Figure 1. Control scheme of the proposed concept for frequency regulation by PMSG-WTG

As described, the rotor speed of a PMSG-WTG depends on the wind speed conditions. For this purpose, the limits of the rotor speed operating range are defined as:

$$\begin{cases} \omega_{r,\min} = \dfrac{V_{w-cutin}}{V_{w-rated}}\omega_{r,rated} \\ \omega_{r,\min}^* = \omega_{r,\min} + \omega_{r,mgn} \end{cases} \tag{9a}$$

$$\omega_{r,\max}^* = \omega_{r,rated} + \omega_{r,mgn} \tag{9b}$$

In (9), the superscript * represents the rotor speed during system disturbances when the proposed design is activated. It is assumed that the normal operating range of the WT rotor speed varies between [$\omega_r^*{}_{,min}$, $\omega_{r,rated}$]. However, the dynamic rotor speed is allowed to vary within the range [$\omega_{r,min}$, $\omega_r^*{}_{,max}$]. If these limits are violated, the WT protection system is triggered. The allowable speed margin ($\omega_{r,mgn}$) is restricted to 0.1 p.u. for the normal operating range of the WT rotor speed.

The gain of the controller (K_ω) is determined considering the practical characteristics of the WTG and dynamic frequency limitations. In this study, the factor 'K_ω' is calculated by the worst-case analysis. It is assumed that the system frequency should not exceed ±1% during a system disturbance, which is also encouraged by IEEE1547 [41]. For simplicity, the system frequency was maintained at 50 Hz (1.0 p.u.). In the worst case, the frequency drops from 1.0 p.u. to 0.99 p.u. or rises from 1.0 p.u. to 1.01 p.u. At the same time, if the rotor speed is initially at $\omega_r^*{}_{,min}$ or $\omega_{r,rated}$, the inertial support is activated, and the rotor speed during disturbance deviates from $\omega_r^*{}_{,min}$ to $\omega_{r,min}$ or from $\omega_{r,rated}$ as $\omega_r^*{}_{,max}$. Thus, the maximum gain can be expressed as:

$$K_{\omega,\max} = \frac{\omega_{r,mgn(p.u.)}}{\Delta f_{g,\max(p.u.)}} \tag{10}$$

In (10), $\Delta f_{g,max}$ represents the maximum allowable frequency deviation. When the frequency deviation is detected, a step-change in the rotor-speed reference is provided by the proposed design. This will be beneficial as it immediately triggers KE release or KE store operations. A schematic of the proposed frequency regulation design applied to PMSG-WTG is shown in Fig. 1. This figure

indicates that when the rotor speed touches its limits [$\omega_{r,min}$, $\omega_{r\ ,max}^{*}$], the output signal of the block will be zero because of the AND operator.

K_ω refers to the performance indicator of PMSG-WTG in providing frequency support. The higher the value of K_ω, the larger the frequency regulation recognized by the WTG. Interestingly, despite the WTG rotor speed touching its leading edges ($\omega_{r\ ,min}^{*}$, $\omega_{r,rated}$) at frequency disturbance events, the rotor speed will not violate its dynamic limits [$\omega_{r,min}$, $\omega_{r\ ,max}^{*}$] because of the continuous changes in the rotor-speed reference. Therefore, a margin for the system operation would be provided, ultimately expanding the stability margin. A schematic of the MSC control with the proposed control design for frequency support is presented in Fig. 2. A detailed control structure of the WTG is omitted here. However, it can be found in [10-11], [42-43].

If the system is running at speeds greater than its defined limits, the value of K_ω should be small; otherwise, there is a strong possibility that the rotor speed exceeds its dynamic range. Therefore, within its normal operating range, a higher K_ω value is suitable for the rotor speed. However, a low K_ω value is beneficial when the system is operating at the vertexes of speed limits and decreases even more if the rotor speed tends to increase or decrease before exceeding its dynamic limits.

Notably, there will be an energy loss, regardless of the type of inertial control applied. For instance, when the stored KE of the WTG is extracted subject to a load disturbance, the rotor speed slows down, which causes the WT to deviate from its optimum operation and ultimately reduces its conversion efficiency.

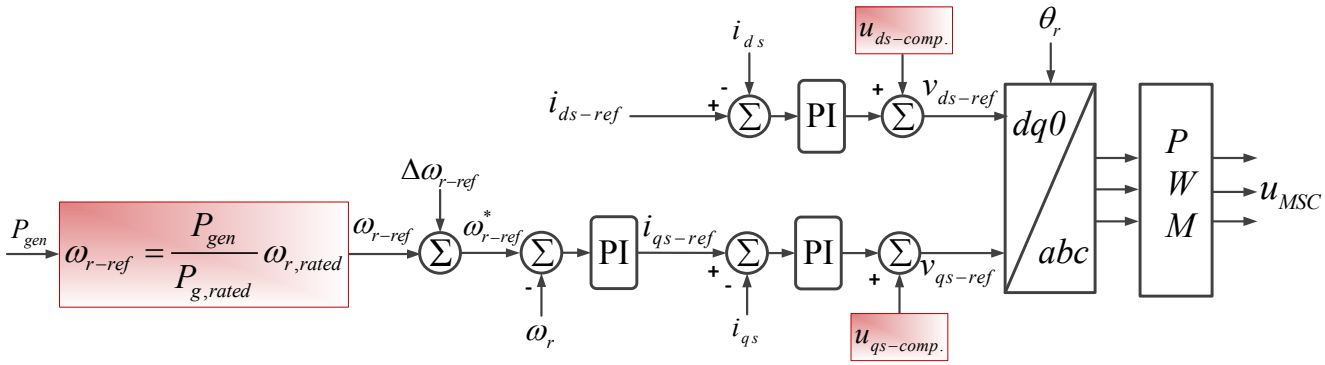

Figure 2. Schematic of the MSC including the proposed control signal for frequency regulation

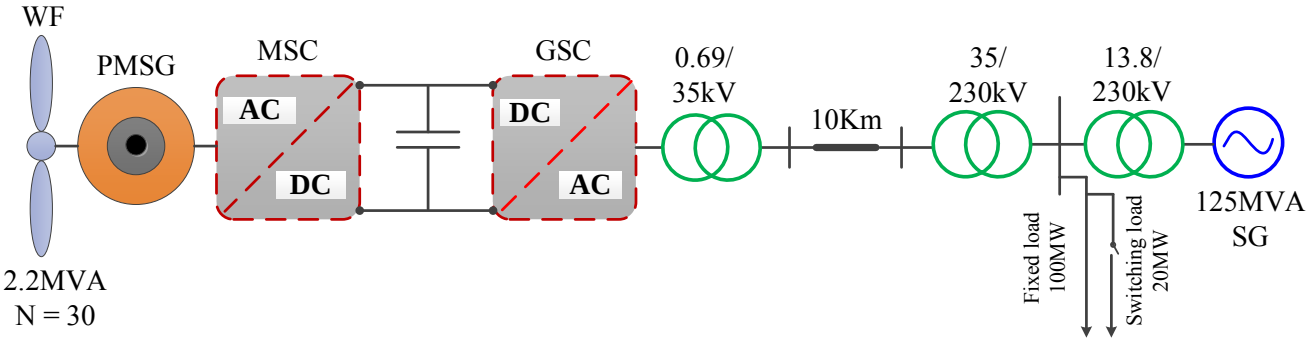

Figure 3. Single-line diagram of the simulated power system

However, additional energy must be provided during voltage recovery to accelerate the WT rotor back to its initial value.

The analytical expressions for *dq* stator-current references are expressed as:

$$i_{ds-ref} = 0 \tag{11a}$$

$$i_{ds-ref} = \left(k_{pw} + \frac{k_{iw}}{s}\left(w^{*}_{r-ref} - \omega_r\right)\right) \tag{11b}$$

In (11b), $k_{p\omega}$ and $k_{i\omega}$ are the proportional and integral gains of speed PI regulator, respectively. Analytical expressions for control signals of the machine-side converter (MSC) are given by:

$$u_{ds-ref} = \left(k_{pi} + \frac{k_{ii}}{s}\right)\left(i_{ds-ref} - i_{ds}\right) + u_{ds-comp.} \tag{12a}$$

$$u_{qs-ref} = \left(k_{pi} + \frac{k_{ii}}{s}\right)\left(i_{qs-ref} - i_{qs}\right) + u_{qs-comp.} \tag{12b}$$

where k_{pi} and k_{ii} are the proportional and integral gains of current PI regulators, respectively. The *d*- and *q*-axis stator-voltage compensation terms are expressed as:

$$u_{ds-comp.} = -\omega_r L_s i_{qs} \tag{13a}$$

$$u_{qs-comp.} = \omega_r\left(L_s i_{ds} + \psi_{pm}\right) \tag{13b}$$

III. Simulation Results and Discussions

Extensive simulations in MATLAB/Simulink were conducted and are presented in this section to verify the proposed concept of providing support for system frequency regulation from WTG subject to a disturbance explained in Section II. A test system comprising 30 identical WTGs (hereunder referred to as the wind farm (WF)), one SG, and two loads, one fixed and other switchable, was used. Figure 3 presents the single-line diagram of the simulated power system. The important system parameters and the parameters of PI regulators are provided in the Appendix A. The rating of SG was 125 MVA. However, the total capacity of the WF was 60 MVA. Therefore, the penetration

level of wind power was approximately 32.4% for the test system. The AC coupling voltage was set to 230 kV. The rating of the fixed load was 100 MW + 25 MVAR. In contrast, the switchable load is specified as 20 MW + 5 MVAR, which represents 20% of the fixed load.

The simulation results indicate that a smooth transfer of the WF from its normal operation to KE release and absorption is accomplished by the proposed concept. For comparative analyses, a simultaneous control (SC) of the *P*–*f* droop controller and DC-link inertial support was also prepared. Furthermore, the results were obtained when no inertial (NO) support was provided by the WF. However, it will not be fruitful to discuss this in detail. Except for system frequency, there was no change in the WTG quantities, including the rotor speed. The authors have taken extra care not to overinterpret the outcomes of the study presented.

Three cases in respect of wind speed and load demand changes have been considered.

- *Case 1:* High wind speed and load demand decrease
- *Case 2:* Medium wind speed and load demand increase
- *Case 3*: Low wind speed and load demand increase

A. Case 1: High Wind Speed and Load Demand Decrease

To validate the performances of the proposed and SC designs, a switchable load with a capacity of 20 MW + 5 MVAR was suddenly removed from the power system at the time (*t*) = 30 s, which causes a frequency increase, as shown in Fig. 4(a). Before this event, the system frequency was 50 Hz, and the rotor speed was approximately 2.347 rad/s, whereas the wind speed was 12 m/s. It is visible from Fig. 4(a) that the frequency peaks during this event are lower than those without inertial support and are 50.48 Hz by proposed design, 50.53 Hz by 'SC,' and 50.55 Hz by 'NO', which shows that the proposed design is faster as the frequency excursions are arrested earlier than those with SC.

The sudden power imbalance accelerates the rotor speed from 2.347 to 2.47 rad/s in the case of the proposed design, whereas this value increases to 2.405 rad/s from its initial value when the SC is applied (see Fig. 4(b)), which means that the proposed design absorbs additional power for frequency regulation. The active power of the WF (P_{MSC}) will be lower (approximately 54.42 MW) from its initial value (59.4 MW) with the application of the proposed design; consequently, the active power through the grid-side converter (P_{GSC}) delivered to the system, that is, 53.86 MW, as shown in Figs. 4(d) and 4(e). In contrast, P_{GSC} via SC is nearly 57.2 MW.

Relays ($R_{\omega 1}$ and $R_{\omega 2}$) activations are realized according to the system frequency deviations, and their on/off statuses are specified in the proposed control design (see Fig. 1). Figure 4(c) presents the generator-torque dynamics, which decrease at the moment when the frequency exceeds its upper limit, and both control schemes are activated. The magnitude of the available torque of the proposed design is far below that of the SC. The DC-link only absorbs energy if the SC is applied, as indicated by the DC-link voltage changes in Fig. 4(f).

During the recovery stage, the frequency starts to drop, and the frequency nadirs of the 'proposed design,' 'SC,' and 'NO' are 49.90, 49.75, and 49.63 Hz, respectively. The high acceleration of the rotor speed via the proposed concept (see Fig. 4(b)) prevents the frequency drop.

Given the above analysis, it is clear that the proposed control provided a satisfactory response in earlier arresting the system frequency excursions compared to the SC when subject to the same system disturbance. It effectively reduced the dynamic frequency deviations and absorbed more active power from the system than that with the SC. Thus, the superior performance of the proposed control concept is ensured.

B. Case 2: Medium Wind Speed and Load Demand Increase

In this case, a switchable load of capacity 20 MW + 5 MVAR was suddenly added to the power system at *t* = 30 s, which causes a frequency drop, as shown in Fig. 5(a). Before this event, the system frequency was 50 Hz, and the rotor speed was approximately 1.858 rad/s; however, the wind speed was 9.5 m/s. As shown in Fig. 5(a), the frequency nadirs of 'NO,' 'SC,' and 'proposed design' fall to approximately 49.40, 49.44, and 49.50 Hz, respectively. In this regard, the rotor speed will decrease to supply the stored KE from the WF to the system. With the application of the proposed design, the speed drops to nearly 1.706 rad/s, which is significantly lower than the speed dynamics (1.807 rad/s) via the SC scheme (see Fig. 5(b)), implying that the proposed design delivers more power to the system for frequency regulation.

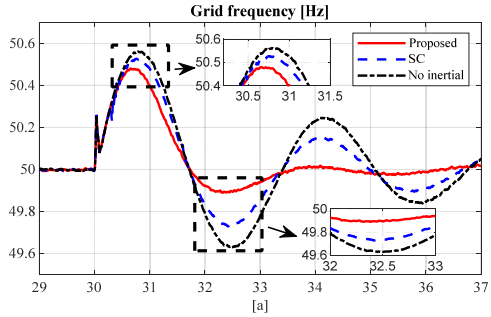

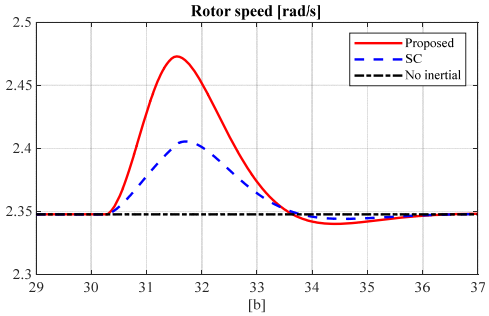

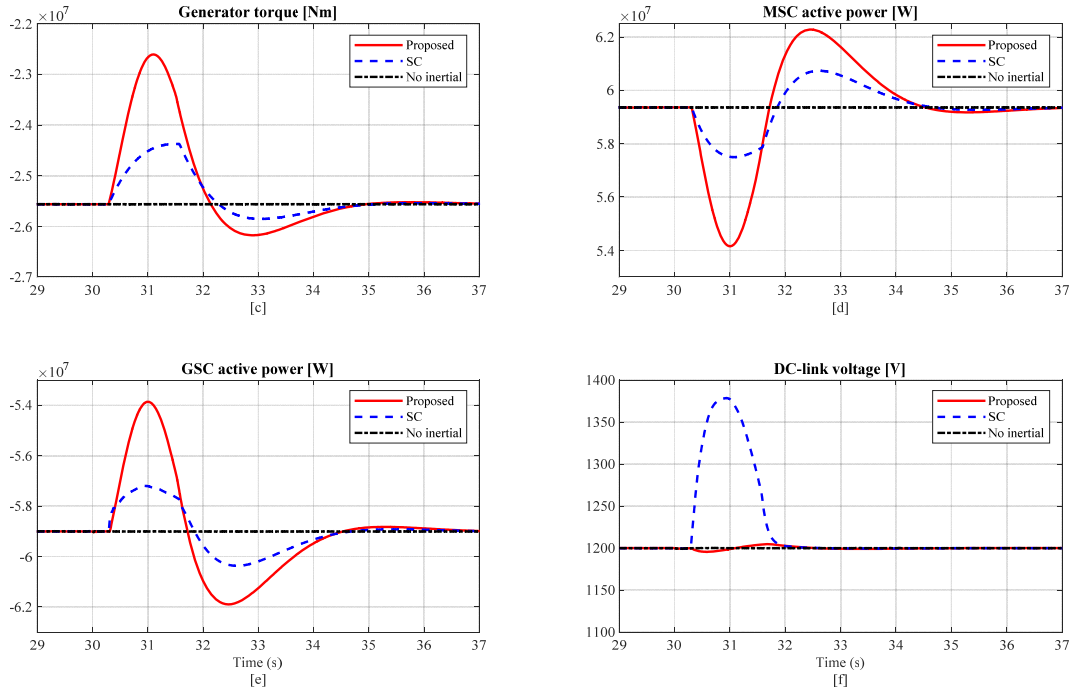

Figure 4. Simulation results of the test system for Case-1

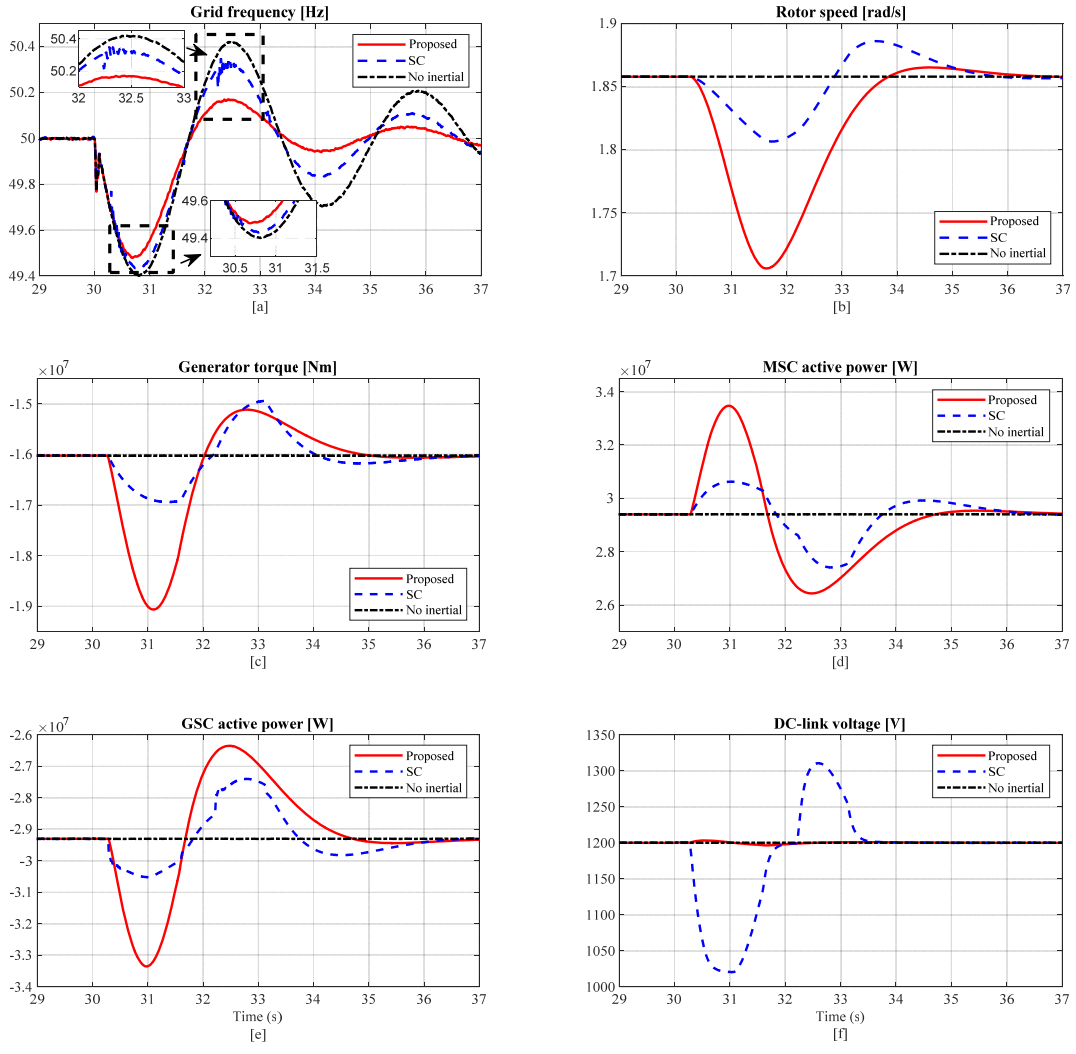

Figure 5. Simulation results of the test system for Case-2

It can be seen from Figs. 5(d) and 5(e) that it transfers approximately 4.05 extra power to the system. However, the SC design only provides 1.22 extra power, which is considerably lower than that of the proposed design. The magnitude of the available torque is far below that of the SC than with the proposed design. The DC-link stored energy is

only available for frequency support if the SC is applied, indicated by the DC-link voltage changes in Fig. 5(f).

During the recovery phase, the frequency increases. As far as the rotor-speed dynamics via the proposed design are concerned, it will continue to decrease despite the increase in frequency being detected because the relay ($R_{\omega 1}$) will remain active until the frequency is below 49.9 Hz, which is beneficial for improving the second-frequency nadir. The system frequency does not touch the threshold required to trigger $R_{\omega 2}$ because of the rotor speed dynamics. In the absence of the designed control output, when the frequency exceeds 49.9 Hz, the rotor speed increases slowly and takes more time to regain its initial state.

The SG mechanical power (not shown here) begins to increase to compensate for load deficiency. As more power (comprising wind power and stored KE) is delivered to the grid during frequency drop, additional power is required to speed up the WTGs to achieve their initial values. In this regard, only a portion of the available wind power is supplied to the grid. It is observed that during the recovery phase, the frequency increase is higher, that is, 50.35 Hz in the case of SC design compared to those obtained from the proposed design (about 50.15 Hz), whereas it is 50.42 Hz when no inertial control is applied.

C. Case 3: Low Wind Speed and Load Demand Increase

The output power of a WF depends on the wind speed, as previously mentioned. When the wind speed was low, the power transferred to the power system decreased. The wind speed was set at 6.5 m/s, and the rotor speed was initially 1.267 rad/s according to wind speed. This subsection focuses on highlighting the availability of KE despite the low wind speed conditions subject to an increase in load demand. Initially, the WF provides approximately 9.30 MW (see Fig. 6(e)). An event in which an extra load of capacity 18 MW + 5 MVAR is suddenly added at t = 30 s is simulated to show the ability of the WF to provide system frequency regulation, whereas the initial load was 100 MW + 20 MVAR, resulting in a decrease in the frequency, as shown in Fig. 6(a). The frequency nadirs achieved by 'proposed design,' 'SC,' and 'NO' controls are about 49.50, 49.47, and 49.45 Hz, respectively, subject to the load disturbance.

A drop in rotor speed, via the proposed control, from 1.267 to 1.131 rad/s indicates a greater availability of KE than that in the SC design, in which the speed drops to 1.237 rad/s. Conversely, the rotor speed remains the same when no inertial support is provided (see Fig. 6(b)). As shown in Fig. 6(e), more active power from the WF is delivered to the power system after the load disturbance using the proposed design because the reduction in rotor speed enhances the KE. The powers delivered to the 'proposed design' and 'SC' systems are 11.8 and 9.9 MW, respectively.

During the recovery phase, the frequency increases. As in Case 2 (see Subsection III-B), the same rotor speed dynamics are extracted. Frequency nadirs in respect of 'proposed design,' 'SC,' and 'NO' are 50.24, 50.33, and 50.39 Hz, respectively. Signal analyses of the selected variables for all the cases are presented in Table I.

Conclusively, it is found that the proposed control design is more energy-efficient than SC while offering better system frequency regulation at the same time. Furthermore, the proposed design effectively improves the frequency nadir, and its simple implementation will be beneficial for practical applications, particularly with the massive integration of WPPs.

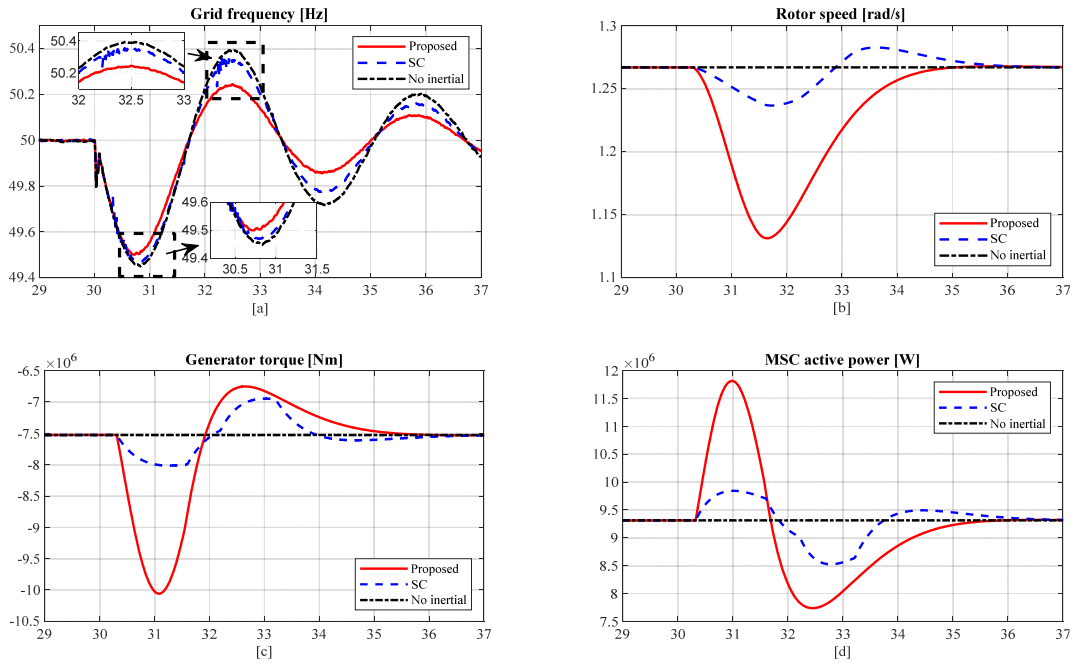

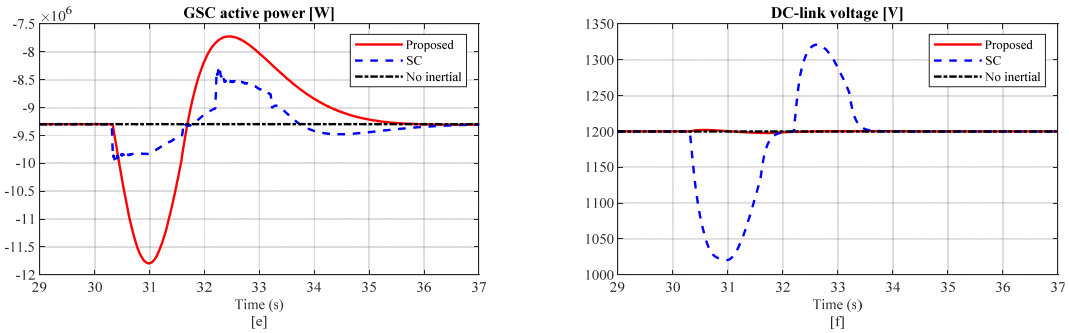

Figure 6. Simulation results of the test system for Case-3

TABLE I. COMPARATIVE RESULTS OF THE SIMULATED CASES

Maximum/Minimum values of the selected variables	During system disturbance			During recovery stage		
	NO	SC	Proposed	NO	SC	Proposed
Case-1						
Frequency (Hz)	50.55	50.53	50.48	49.63	49.75	49.90
Rotor speed (rad/s)	2.347	2.405	2.47	2.347	2.344	2.34
Active power (P_{GSC}) (MW)	59.0	57.2	53.86	59.0	60.37	61.90
Case-2						
Frequency (Hz)	49.40	49.44	49.50	50.42	50.35	50.15
Rotor speed (rad/s)	1.858	1.807	1.706	1.858	1.886	1.865
Active power (P_{GSC}) (MW)	29.30	30.52	33.35	29.30	27.40	26.35
Case-3						
Frequency (Hz)	49.45	49.47	49.50	50.39	50.33	50.24
Rotor speed (rad/s)	1.267	1.237	1.131	1.267	1.283	1.267
Active power (P_{GSC}) (MW)	9.29	9.95	11.80	9.29	8.35	7.725

IV. CONCLUSION

This paper discussed the transient problem of a grid-connected wind-driven PMSG subject to load disturbances under different wind speeds. It proposed a control concept based on modifying the WTG control design, enabling frequency support from WTGs by utilizing their stored KE. Under this design, the KE release and absorption were triggered by directly controlling the rotor-speed reference by absorbing or releasing KE from or to the system when exposed to load demand changes. The concept used a direct relation between the rotor-speed reference and system frequency deviations to enable the system transient performance.

The superior performance of the proposed solution was confirmed through simulations. A control performance comparison with the SC of the *P–f* droop controller and DC-link inertial support ensured a satisfactory response in earlier arresting the system frequency excursions compared to the SC subject to the same system disturbance. It effectively reduced the dynamic frequency deviations and provided more active power to the system from the WF than that with the SC. Thus, the superior performance of the proposed control concept was guaranteed. It is hoped that this study will lead to new insights into using the available potentials of WTGs to deal with the frequency issue subject to load changes. The following conclusions were drawn.

The proposed solution was effective in providing frequency support, subject to load demand changes. The capacity of the variable-speed WTG supported frequency regulation by applying the proposed control concept, that is, utilizing the KE stored in their rotating bodies. The proposed concept effectively accelerates or decelerates the rotor speed.

APPENDIX A

Wind turbine: rated power: 2.0 MW; air density: 1.225 kg/m^3; radius: 14.26 m; rated wind speed: 12 m/s; rated rotor speed: 2.34 rad/s; optimum tip-speed ratio: 8.1; maximum power coefficient: 0.48; No. of wind turbines: 30.

PMSG: rated power: 2.2 MW; pole pair: 26 Nos.; stator-winding resistance: 0.8 mΩ; stator-winding inductance: 1.57 mH; rotational inertia: 500,000 kg·m^2.

Converters: DC-link voltage reference: 1200 V; DC-link capacitance: 20 mF; grid-side filter resistance: 12.6 mΩ, grid-side filter inductance: 0.3 mH.

Transmission line: line length = 10 km; line resistance: 0.1153 mΩ/km; line reactance: 1.05 mH/km.

SG: rated power: 125 MVA; line-to-line voltage: 13.8 kV; x_d, x_d', x_d'' = 2.24 p.u., 0.17 p.u., 0.12 p.u.; x_q, x_q', x_l = 1.02 p.u., 0.13 p.u., 0.08 p.u.; T_d, T_d', T_q'' = 0.012 s, 0.003 s, 0.003 s; inertia constant: 3 s.

Diesel governor setting: T_1: 0.02 s; T_2: 5 s; K = 20.

AVR setting: exciter regulator gain: 300; exciter time constant: 0.001 s.

TABLE II. PARAMETERS OF PI CONTROLLERS

Controller	K_p	K_i
Speed controller	300	3000
Current controllers	0.4	12

NOMENCLATURE

Abbreviations:

DFIG	Doubly fed induction generator
ESD	Energy storage device
GSC	Grid-side converter
KE	Kinetic energy
MPPT	Maximum power point tracking
MSC	Machine-side converter
NO	No inertial support
PAC	Pitch-angle control
PEI	Power-electronic interface
PI	Proportional-integral
PMSG	Permanent-magnet synchronous generator
SC	Simultaneous control
SG	Synchronous generator
VSWT	Variable-speed wind turbine
WECS	Wind energy conversion system
WF	Wind farm
WPPs	Wind power plants
WT	Wind turbine
WTG	Wind turbine generator

Variables:

ω_r	Rotor speed
$\omega_{r,rated}$	Rated rotor speed
$\omega_{r\text{-}ref}$	Rotor-speed reference
$\omega_{r,min}$	Minimum rotor speed
$\omega_{r,max}$	Maximum rotor speed
$V_{w\text{-}cutin}$	Cut-in wind speed
$V_{w\text{-}rated}$	Rated wind speed
$i_{ds\text{-}ref}$	Direct (d) axis stator-current reference
i_{ds}	d-axis stator current
$i_{qs\text{-}ref}$	Quadrature (q) axis stator-current reference
i_{qs}	q-axis stator current
$u_{ds\text{-}ref}$	d-axis stator-voltage reference
$u_{qs\text{-}ref}$	q-axis stator-voltage reference
$u_{ds\text{-}comp.}$	d-axis stator-voltage compensation term
$u_{qs\text{-}comp.}$	q-axis stator-voltage compensation term
L_s	Stator inductance
ψ_{pm}	Flux provided by permanent magnets
T_t	Turbine torque
T_e	Generator electrical torque
J_T	WTG's inertia
P_{KE}	Inertial power
k_p	Proportional gain of PI regulator
k_i	Integral gain of PI regulator
S	Rated power of the electric machine
ρ	Air density
R	Rotor radius
$C_{p,opt}$	Optimal power conversion efficiency
λ_{opt}	Optimal tip-speed ratio
K_{opt}	Design parameter
P_{gen}	Generator output power
$P_{g,rated}$	Rated generator power
f_g	Rated system frequency
$f_{g,meas}$	Measured system frequency

REFERENCES

[1] M. A. S. Ali, "LMI-based state feedback control structure for resolving grid connectivity issues in DFIG-based WT systems," Eng, vol. 2, no. 4, pp. 562-591, 2021. doi:10.3390/eng2040036

[2] S. Daniar, F. Aminifar, M. R. Hesamzadeh, H. Lesani, "Optimal controlled islanding considering frequency-arresting and frequency-stabilising constraints: A graph theory-assisted approach," IET Generation, Transmission & Distribution, vol. 15, no. 14, pp. 1–17, 2021. doi:10.1049/gtd2.12154

[3] Q. C. Zhong, "Power-electronics-enabled autonomous power systems: Architecture and technical routes," IEEE Transactions on Industrial Electronics, vol. 64, no. 7, pp. 5907–5918, 2017. doi:10.1109/TIE.2017.2677339

[4] Y. Wu, W. Yang, Y. Hu, P. Q. Dzung, "Frequency regulation at a wind farm using time-varying inertia and droop controls," IEEE Transactions on Industry Applications, vol. 55, no. 1, pp. 213–224, 2019. doi:10.1109/TIA.2018.2868644

[5] Z. Wang, W. Wu, "Coordinated control method for DFIG-based wind farm to provide primary frequency regulation service," IEEE Transactions on Power Systems, vol. 33, no. 3, pp. 2644–2659, 2018. doi:10.1109/TPWRS.2017.2755685

[6] Y. Zhang, A. M. Melin, S. M. Djouadi, M. M. Olama, K. Tomsovic, "Provision for guaranteed inertial response in diesel wind systems via model reference control," IEEE Transactions on Power Systems, vol. 33, no. 6, pp. 6557–6568, 2018. doi:10.1109/TPWRS.2018.2827205

[7] X. Xi, H. Geng, G. Yang, S. Li, F. Gao, "Torsional oscillation damping control for DFIG-based wind farm participating in power system frequency regulation," IEEE Transactions on Industry Applications, vol. 54, no. 4, pp. 3687–3701, 2018. doi:10.1109/TIA.2018.2814559

[8] X. Xi, H. Geng, G. Yang, S. Li, F. Gao, "Two-level damping control for DFIG-based wind farm providing synthetic inertial service," IEEE Transactions on Industry Applications, vol. 54, no. 2, pp. 1712–1723, 2018. doi:10.1109/TIA.2017.2765298

[9] M. Raffaele, R. Silvia, M. Canevese, "Fast frequency regulation and synthetic inertia in a power system with high penetration of renewable energy sources: Optimal design of the required quantities," Sustainable Energy, Grids and Networks, vol. 24, p. 100407, 2020. doi:10.1016/j.segan.2020.100407

[10] M. A. S. Ali, K. K. Mehmood, C. H. Kim, "Full operational regimes for SPMSG-based WECS using generation of active current references," International Journal of Electrical Power & Energy Systems, vol. 112, pp. 428–441, 2019. doi:10.1016/j.ijepes.2019.05.028

[11] M. A. S. Ali, K. K. Mehmood, S. Baloch, C. H. Kim, "Wind-speed estimation and sensorless control for SPMSG-based WECS using LMI-based SMC," IEEE Access, vol. 8, pp. 26524–26535, 2020. doi:10.1109/ACCESS.2020.2971721

[12] D. Zouheyr, B. Lotfi, B. Abdelmadjid, "Improved hardware implementation of a TSR based MPPT algorithm for a low cost connected wind turbine emulator under unbalanced wind speeds," Energy, vol. 232, p. 121039, 2021. doi:10.1016/j.energy.2021.121039

[13] M. A. S. Ali, K. K. Mehmood, C. H. Kim, "Power system stability improvement through the coordination of TCPS-based damping controller and power system stabilizer," Advances in Electrical and Computer Engineering, vol. 17, no. 4, pp. 27–36, 2017. doi:10.4316/AECE.2017.04004

[14] S. Wang, J. Hu, X. Yuan, L. Sun, "On inertial dynamics of virtual-synchronous-controlled DFIG-based wind turbines," IEEE Transactions on Energy Conversion, vol. 30, no. 4, pp. 1691–1702, 2015. doi:10.1109/TEC.2015.2460262

[15] Y. Fu, Y. Wang, X. Zhang, "Integrated wind turbine controller with virtual inertia and primary frequency responses for grid dynamic frequency support," IET Renewable Power Generation, vol. 11 no. 8, pp. 1129–1137, 2017. doi:10.1049/iet-rpg.2016.0465

[16] Y. Li, Z. Xu, J. Zhang, K. P. Wong, "Variable gain control scheme of DFIG-based wind farm for over-frequency support,". Renewable Energy, vol. 120, pp. 379–391, 2018. doi:10.1016/j.renene.2017.11.055

[17] Y. Li, Z. Xu, J. Zhang, K. P. Wong, "Advanced control strategies of PMSG-based wind turbines for system inertial support," IEEE Transactions on Power Systems, vol. 32, no. 4, pp. 3027–3037, 2017. doi:10.1109/TPWRS.2016.2616171

[18] H. Ye, W. Pei, Z. Qi, "Analytical modeling of inertial and droop responses from a wind farm for short-term frequency regulation in power systems," IEEE Transactions on Power Systems, vol. 31, no. 5, pp. 3414–3423, 2016. doi:10.1109/TPWRS.2015.2490342

[19] J. Van de Vyver, J. D. M. Kooning, B. Meersman, L. Vandevelde, T. L. Vandoorn, "Droop control as an alternative inertial response strategy for the synthetic inertia on wind turbines," IEEE Transactions on Power Systems, vol. 31, no. 2, pp. 1129–1138, 2016. doi:10.1109/TPWRS.2015.2417758

[20] M. Kayikci, J. V. Milanovic, "Dynamic contribution of DFIG-based wind plants to system frequency disturbances," IEEE Transactions on Power Systems, vol. 24, no. 2, pp. 859–867, 2009. https://doi:10.1109/TPWRS.2009.2016062

[21] W. Yi, M. Jianhui, Z. Xiangyu, X. Lie, "Control of PMSG-based wind turbines for system inertial response and power oscillation damping," IEEE Transactions on Sustainable Energy, vol. 6, no. 2, pp. 565–574, 2015. doi:10.1109/TSTE.2015.2394363

[22] X. Zhang, X. Zha, S. Yue, Y. Chen, "A frequency regulation for wind power based on limited over-speed de-loading curve partitioning," IEEE Access, vol. 6, pp. 22938–22951, 2018. doi:10.1109/ACCESS.2018.2825363

[23] Y. Li, Z. Xu, J. Zhang, H. Yang, K. P. Wong, "Variable utilization level scheme for load-sharing control of wind farm," IEEE Transactions on Energy Conversion, vol. 33, no. 2, pp. 856–868, 2018. doi:10.1109/TEC.2017.2765399

[24] P. Li, W. Hu, R. Hu, Q. Huang, J. Yao, Z. Chen, "Strategy for wind power plant contribution to frequency control under variable wind speed," Renewable Energy, vol. 130, pp. 1226–1236, 2019. doi:10.1016/j.renene.2017.12.046

[25] X. Lyu, J. Zhao, Jia Y. Jia, Z. Xu, K. P. Wong, "Coordinated control strategies of PMSG-based wind turbine for smoothing power fluctuations," IEEE Transactions on Power Systems, vol. 34, no. 1, pp. 391–401, 2019. doi:10.1109/TPWRS.2018.2866629

[26] A. Uehara, A. Pratap, T. Goya, T. Senjyu, A. Yona, N. Urasaki, T. Funabashi, "A coordinated control method to smooth wind power fluctuations of a PMSG-based WECS," IEEE Transactions on Energy Conversion, vol. 26, no. 2, pp. 550–558, 2011. doi:10.1109/TEC.2011.2107912

[27] D. Gautam, L. Geol, R. Ayyanar, V. Vittal, T. Harbour, "Control strategy to mitigate the impact of reduced inertia due to doubly fed induction generators on large power systems," IEEE Transactions on Power Systems, vol. 26, no. 1, pp. 214–224, 2011. doi:10.1109/TPWRS.2010.2051690

[28] X. Zeng, T. Liu, S. Wang, Y. Dong, Z. Chen, "Comprehensive coordinated control strategy of PMSG-based wind turbine for providing frequency regulation services," IEEE Access, vol. 7, pp. 63944–63953, 2019. doi:10.1109/ACCESS.2019.2915308

[29] H. Shao, X. Cai, Z. Li, D. Zhou, S. Sun, L. Guo, Y. Cao, F. Rao, "Stability enhancement and direct speed control of DFIG inertia emulation control strategy," IEEE Access, vol. 7, pp. 120089–120105, 2019. doi:10.1109/ACCESS.2019.2937180

[30] J. Zhao, X. Lyu, Y. Fu, X. Hu, F. Li, "Coordinated microgrid frequency regulation based on DFIG variable coefficient using virtual inertia and primary frequency control," IEEE Transactions on Energy Conversion, vol. 31, no. 3, pp. 833–845, 2016. doi:10.1109/TEC.2016.2537539

[31] K. Visscher, S. W. H. De Haan, "Virtual synchronous machine (VSG's) for frequency stabilization in future grids with a significant share of decentralized generation," In: IET-CIRED Seminar Smart-Grid Distribution; Germany: 1–4, 2008

[32] T. Kerdphol, F. S. Rahman, M. Watanabe, et al., "Small-signal analysis of multiple virtual synchronous machines to enhance frequency stability of grid-connected high renewables," IET Generation, Transmission & Distribution, vol. 15, no. 8, pp. 1273–1289, 2021. doi:10.1049/gtd2.12101

[33] Q. C. Zhong, G. Weiss, "Synchronverters: inverters that mimic synchronous generators," IEEE Transactions on Industrial Electronics, vol. 58, no. 4, pp. 1259–1267, 2011. doi:10.1109/TIE.2010.2048839

[34] M. Fazeli, G. M. Asher, C. Klumpner, L. Yao, M. Bazargan, "Novel integration of wind generator-energy storage systems within microgrids," IEEE Transactions on Smart Grid, vol. 3, no. 2, pp. 728–737, 2012. doi:10.1109/TSG.2012.2185073

[35] M. A. S. Ali, K. K. Mehmood, J. K. Park, C. H. Kim, "Battery energy storage system-based stabilizers for power system oscillations damping," Journal of the Korean Institute of Illuminating and Electrical Installation Engineers, vol. 10, pp. 75–84, 2016. doi:10.5207/JIEIE.2016.30.10.075

[36] J. Zhu, X. Lyu, Y. Fu, X. Hu, F. Li, "Synthetic inertia control strategy for doubly fed induction generator wind turbine generators using lithium-ion supercapacitors," IEEE Transactions on Energy Conversion, vol. 33, no. 2, pp. 773–783, 2018. doi:10.1109/TEC.2017.2764089

[37] W. Xing, H. Wang, L. Lu, X. Han, K. Sun, M. Ouyang, "An adaptive virtual inertia control strategy for distributed battery energy storage system in microgrid," Energy, vol. 233, p. 121155, 2021. doi:10.1016/j.energy.2021.121155

[38] M. A. S. Ali, K. K. Mehmood, J. S. Kim, C. H. Kim, "ESD-based crowbar for mitigating DC-link variations in a DFIG-based WECS," 2019 International Conference on Power Systems Transients (IPST), Perpignan, 2019, pp. 1–6

[39] Y. Zuoa, Z. Yuana, F. Sossanb, A. Zecchinoa, R. Cherkaouia, M. Paolonea, "Performance assessment of grid-forming and grid-following converter-interfaced battery energy storage systems on frequency regulation in low-inertia power grids," Sustainable Energy, Grids and Networks, vol. 27, p. 100496, 2021. doi:10.1016/j.segan.2021.100496

[40] C. Parthasarathy, H. Hafezi, H. Laaksonen, "Integration and control of lithium-ion BESSs for active network management in smart grids: Sundom smart grid backup feeding case," Electrical Engineering, vol. 33, no. 6, pp. 859–867, 2021. doi:10.1007/s00202-021-01311-8

[41] IEEE application guide for interconnecting distributed resources with electric power systems, IEEE Standard 1547.2TM, 2008

[42] M. A. S. Ali, K. K. Mehmood, S. Baloch, C. H. Kim, "Modified rotor-side converter control design for improving the LVRT capability of a DFIG-based WECS," Electric Power Systems Research, vol. 186, p. 106403, 2020. doi:10.1016/j.epsr.2020.106403

[43] M. A. S. Ali, "Utilizing active rotor-current references for smooth grid connection of a DFIG-based wind-power system," Advances in Electrical and Computer Engineering, vol. 21, no. 4, pp. 91–98, 2020. doi:10.4316/AECE.2020.04011